



Crystal structures of *Escherichia coli* glucokinase and insights into phosphate binding

Joseph Andrews,^a Joshua Sakon^{a,b*} and Chenguang Fan^{a,b*}^aDepartment of Chemistry and Biochemistry, University of Arkansas at Fayetteville, Fayetteville, AR 72701, USA, and^bCell and Molecular Biology Program, University of Arkansas at Fayetteville, Fayetteville, AR 72701, USA. *Correspondence e-mail: jsakon@uark.edu, cf021@uark.edu

Received 7 April 2025

Accepted 19 June 2025

Edited by R. Sankaranarayanan, Centre for Cellular and Molecular Biology, Hyderabad, India

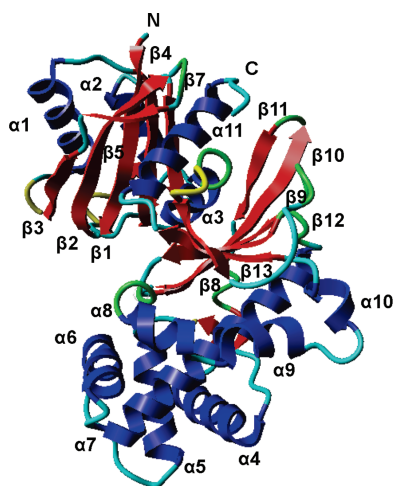
Keywords: glucokinases; hexokinases; phosphate binding; sulfate binding.**PDB references:** *Escherichia coli* glucokinase, 9duc; with glucose bound, 9dvz**Supporting information:** this article has supporting information at journals.iucr.org/f

Here, we report the crystal structure of *Escherichia coli* glucokinase (GLK), which has phosphate bound in the cleft between the α and β domains adjacent to the active site. A ternary complex consisting of GLK, glucose and phosphate is also reported in this work. Diffraction data were collected at 2.63 Å resolution for the phosphate-bound form ($R_{\text{work}}/R_{\text{free}} = 0.191/0.230$) and at 2.54 Å resolution for the ternary complex ($R_{\text{work}}/R_{\text{free}} = 0.202/0.258$), both at 297 K. A B -factor analysis of the phosphate-bound GLK structure revealed consistently lower values for phosphate-interacting basic residues in the $\alpha 4$, $\alpha 5$ and $\alpha 9$ helices, while significant root-mean-square deviation (r.m.s.d.) spikes indicated flexibility in regions preceding $\beta 1$ and within the loop between the $\beta 5$ and $\beta 6$ sheets of the α domain. In the ternary complex, phosphate is bound adjacent to glucose, and the B factors for the $\alpha 4$, $\alpha 5$ and $\alpha 9$ helices were further reduced, while r.m.s.d. spikes were observed at the end of the $\beta 10$ sheet and within the $\alpha 6$ helix of the β -domain. This structural characterization suggests that phosphate could influence the activity of GLK by altering glucose binding and modulating interactions with a loop-interacting regulatory protein.

1. Introduction

Glucokinase (GLK) catalyzes the first reaction in the glycolytic pathway and is a target for regulation in a wide range of organisms. GLKs are divided into three families based on sequence identities. Group I GLKs comprise ADP- and ATP-dependent GLKs from archaea and a small selection of eukaryotes (Sakuraba *et al.*, 2004; Ronimus & Morgan, 2004). Group II GLKs are ATP-dependent enzymes that lack the classical repressor open reading frame kinase (ROK) sequence motif and contain more than 50 partial and complete protein sequences, including *Escherichia coli* GLK (ecGLK; Titgemeyer *et al.*, 1994; Meyer *et al.*, 1997). Group III GLKs comprise ATP-dependent GLKs from bacteria and archaea which possess the ROK sequence motif (Hansen *et al.*, 2002; Hansen & Schönheit, 2003; Scorpio *et al.*, 2004).

In a previous structural study, apo ecGLK crystals were obtained using the vapor-diffusion method (Lunin *et al.*, 2004). The resulting crystal unit-cell dimensions are $a = b = 81.5$, $c = 234.7$ Å in space group $P4_32_12$, which includes two molecules in the asymmetric unit. EcGLK–glucose complex crystals were also produced using the vapor-diffusion method with 2 mM glucose. These ecGLK–glucose crystals exhibited unit-cell dimensions $a = 78.416$, $b = 53.538$, $c = 90.903$ Å in space group $P12_11$, also containing two molecules in the asymmetric unit. This work showed that during the ecGLK binding-site transformation, the maximum C^α displacement of residues in the small domain on superposing two apo ecGLK monomers was observed at Thr78, indicating that this portion of the loop



OPEN ACCESS

Published under a CC BY 4.0 licence

closes during glucose binding. Superposition of the small domain revealed 320 C α atoms with a root-mean-square deviation (r.m.s.d.) of 1.3 Å. In comparison, the large domain consisted of 186 C α atoms with an r.m.s.d. of 0.38 Å. The binding of glucose was proposed to stabilize the flexible loops of ecGLK, allowing the monomers to adopt a similar conformation. In the absence of glucose, apo ecGLK also demonstrates intrinsic flexibility. During the closure of GLK, residues 73–79 undergo movement, resulting in broken hydrogen bonds between the small and large domains (between Arg16 NE and Thr32 OG1 and between Trp131 O and Glu315 NE2). The closure of the domains generates new hydrogen bonds between Arg16 NE and Asn303 OD, along with Arg16 NH1 and Thr32 OG (Lunin *et al.*, 2004).

To date, there are no ecGLK structures reported together with the other substrate ATP or the product ADP. This work presents the structure of apo ecGLK bound with phosphate and the structure of ecGLK in complex with both glucose and phosphate, implying a role for phosphate in regulation of the GLK activity.

2. Materials and methods

2.1. Purification and crystallization

The expression and purification of ecGLK followed our previous work on this enzyme (Fatema *et al.*, 2024). Briefly, the *E. coli glk* gene was cloned into the pCDF-1b plasmid with a His₆-tag at the C-terminus and was transformed into *E. coli* BL21 (DE3) cells. The expression strain was grown in 400 ml LB medium with 100 µg ml⁻¹ streptomycin at 37°C to an absorbance of between 0.6 and 0.8 at 600 nm. Expression of ecGLK was induced by adding 0.1 mM isopropyl β-D-1-thiogalactopyranoside (IPTG) and incubating at 16°C for an additional 16 h. Cells were harvested and centrifuged at 3000g for 20 min. Cell pellets were stored at -80°C. The purification process involved several steps, including the addition of 12 ml lysis buffer (Tris-HCl pH 7.5, 300 mM NaCl, 20 mM imidazole) to the cell pellet along with 5 µl β-mercaptoethanol, protease inhibitors and nuclease. The mixture was sonicated for 3 min on ice and then centrifuged at 19 000g for 25 min. The supernatant was collected and then filtered using a 0.45 nm filter. The filtered supernatant was added to an affinity chromatography column that contained 2 ml Ni-NTA resin previously equilibrated with 20 ml lysis buffer. The loaded column was washed with 15 ml Tris-HCl pH 7.5 with 50 mM imidazole and 300 mM NaCl, and 2 ml fractions were then eluted using Tris-HCl pH 7.5 with 200 mM imidazole and 300 mM NaCl. SDS-PAGE was used to verify the purity of the ecGLK enzyme. The elution fractions were then added to a PD10 column for desalting using desalting buffer (5 mM Na₂HPO₄, 1 mM NaH₂PO₄ pH 7.5, 10 mM NaCl, 1 mM DTT). The sample was concentrated using a protein concentrator with a cutoff of 100 000 at 3000g until the concentration reached 7–8 mg ml⁻¹. Before crystallization, ecGLK was incubated with 5 mM glucose for 1 h. Crystal screening was initiated using Rigaku Berkeley Screen solutions 1–96. The

Table 1

Crystallographic data and refinement statistics for the X-ray structures.

Values in parentheses are for the highest resolution shell.

	Phosphate–ecGLK	Phosphate–glucose–ecGLK
Data-collection statistics		
Space group	<i>P</i> 4 ₃ 2 ₁ 2	<i>P</i> 2 ₁ 2 ₁ 2 ₁
<i>a</i> , <i>b</i> , <i>c</i> (Å)	82.11, 82.11, 237.93	47.53, 66.28, 207.53
α , β , γ (°)	90.00, 90.00, 90.00	90.00, 90.00, 90.00
Radiation source	Rigaku PhotonJet-S	Rigaku PhotonJet-S
Wavelength (Å)	1.5418	1.5418
Resolution limits (Å)	29.74–2.63 (2.76–2.63)	22.72–2.54 (2.65–2.54)
$R_{\text{merge}}^{\dagger}$ (within <i>I</i> +/ <i>I</i> -)	0.210 (0.902)	0.202 (0.536)
R_{merge} (all <i>I</i> + and <i>I</i> -)	0.216 (0.931)	0.218 (0.592)
$R_{\text{meas}}^{\ddagger}$ (within <i>I</i> +/ <i>I</i> -)	0.233 (1.000)	0.249 (0.657)
R_{meas} (all <i>I</i> + and <i>I</i> -)	0.228 (0.980)	0.243 (0.657)
$R_{\text{p.i.m.}}^{\S}$ (within <i>I</i> +/ <i>I</i> -)	0.100 (0.425)	0.143 (0.375)
$R_{\text{p.i.m.}}$ (all <i>I</i> + and <i>I</i> -)	0.072 (0.304)	0.107 (0.282)
R_{merge} in top intensity bin	0.077 (—)	0.073 (—)
No. of observations	247590 (35037)	111209 (14258)
No. of possible unique observations	25106 (3266)	22512 (2708)
No. of unique observations	25056 (3266)	22445 (2708)
Mean <i>I</i> / σ (<i>I</i>)	9.2 (3.7)	5.5 (2.6)
CC _{1/2}	0.991 (0.743)	0.983 (0.802)
Completeness (%)	99.8 (100)	99.7 (100)
Multiplicity	9.9 (10.7)	5 (5.3)
Mean χ^2	0.95 (0.93)	0.92 (0.96)
Refinement statistics		
Resolution (Å)	29.74–2.63	22.72–2.54
Protein residues	638	638
Solvent molecules	173	176
Phosphate molecules	2	2
R_{free}	0.230	0.257
R_{work}	0.191	0.205
R.m.s.d.		
Bond lengths (Å)	0.002	0.002
Angles (°)	0.507	0.554
Ramachandran plot		
No. of residues	638	638
Most favored regions (%)	93.71	92.87
Allowed regions (%)	6.29	7.13
Mean <i>B</i> factors (Å ²)		
Protein	33.4	23.1
Phosphate	30.0	11.5
Glucose	—	12.9

$\dagger R_{\text{merge}}$, also known as R_{sym} , is a discrepancy index used to measure the equivalence or internal consistency among intensities of equivalent reflections in X-ray crystallography. $\ddagger R_{\text{meas}}$ is a discrepancy index introduced to account for the dependence of R_{merge} (R_{sym}) on the multiplicity, which is the number of equivalent reflections. $\S R_{\text{p.i.m.}}$, or the precision-indicating merging *R* factor, is a discrepancy index introduced to further refine the dependence of R_{meas} on the multiplicity.

sitting-drop vapor-diffusion method was used with two drops: one containing 0.7 µl protein and 1 µl well solution and the second containing 0.5 µl protein and 1 µl well solution. All of the drops were suspended over 35 µl well solution at 293 K. The initial crystallization conditions were refined by systematically altering the buffer, pH and PEG concentrations until diffraction-quality crystals were grown. All the experiments retained the original protein and well solution volume ratio.

2.2. Data collection and processing

Single protein crystals were mounted on a MicroRT-compatible loop holder with a nylon loop (MiTeGen) and then sealed using a MicroRT capillary tube. At the tip of the capillary tube 5 µl mother liquor was present, and the bottom

was sealed with vacuum grease. The crystals were sealed at room temperature and the data were collected at room temperature. X-ray diffraction data were collected using a Rigaku XtaLAB Synergy-S Diffractometer (University of Arkansas, Fayetteville, USA) and a HyPix-6000HE detector. Raw data images were processed using *CrysAlis^{Pro}* and scaled and merged with *AIMLESS*. The structures were determined by the molecular-replacement method using *Phaser* (McCoy *et al.*, 2007) with ecGLK (PDB entry 1q18; Lunin *et al.*, 2004) as the model for the structure of phosphate-bound ecGLK (LLG score 7087.594) and GLK in complex with glucose (PDB entry 1sz2; Lunin *et al.*, 2004) as the model for the structure of the phosphate-bound glucose–ecGLK complex (LLG score 4707.901). Structures were refined using *AutoBuild* for automated model building after molecular replacement (Terwilliger *et al.*, 2008) and *phenix.refine* for model refinement after building (Afonine *et al.*, 2012). The structures were manually adjusted using *WinCoot* (Emsley *et al.*, 2010) for validation/refinement and were submitted to the PDB. The PDB codes for apo ecGLK with phosphate and the phosphate-bound ecGLK–glucose complex are 9duc and 9dvz, respectively. Diffraction data and structure statistics are presented in Table 1. The R_{merge} values for both structures are relatively high, possibly resulting from the high multiplicity observed in the data sets. High multiplicity can inflate R_{merge} values due to the increased number of observations contributing to the averaged intensity of each reflection.

3. Results and discussion

3.1. Apo ecGLK versus phosphate-bound ecGLK: effect of phosphate binding

The phosphate-bound ecGLK crystals were grown in 100 mM Tris–HCl pH 8.5, 200 mM lithium sulfate, 20% (w/v) PEG 5000 MME. The phosphate-bound ecGLK structure from the $P4_32_12$ crystal form was determined by molecular replacement and refined to an R factor of 0.1930 ($R_{\text{free}} = 0.2302$) at a resolution of 2.65 Å. The phosphate-bound complex is composed of a dimer, with each monomer featuring an α/β domain characterized by noncontiguous segments: the small domain (residues 2–110 and 300–321) and the large domain (residues 111–299). The small domain features β -sheets β_1 – β_4 and β_7 , as well as α -helices α_1 – α_3 and α_{11} . The small domain α_3 helix consisting of residues 100–110 links the small and large domains. In contrast, the large domain features β -sheets β_8 – β_{13} and α -helices α_4 – α_{10} . The dimer interface consists of helix α_4 and nearby loops, the C-terminal end of helix α_7 , strand β_{10} and the loop that connects strand β_{10} to strand β_{11} . The phosphate-binding site is found on the edge of the small and large domain cleft outside the α_4 – α_{10} cluster. Comparison between phosphate-bound (PDB entry 9duc) and apo (PDB entry 1q18) ecGLK highlights key structural shifts, including His160 and Arg286 (Fig. 1).

His160 in chain *B* experiences conformational changes from the N atom in its imidazole ring (His160 ND1) forming a

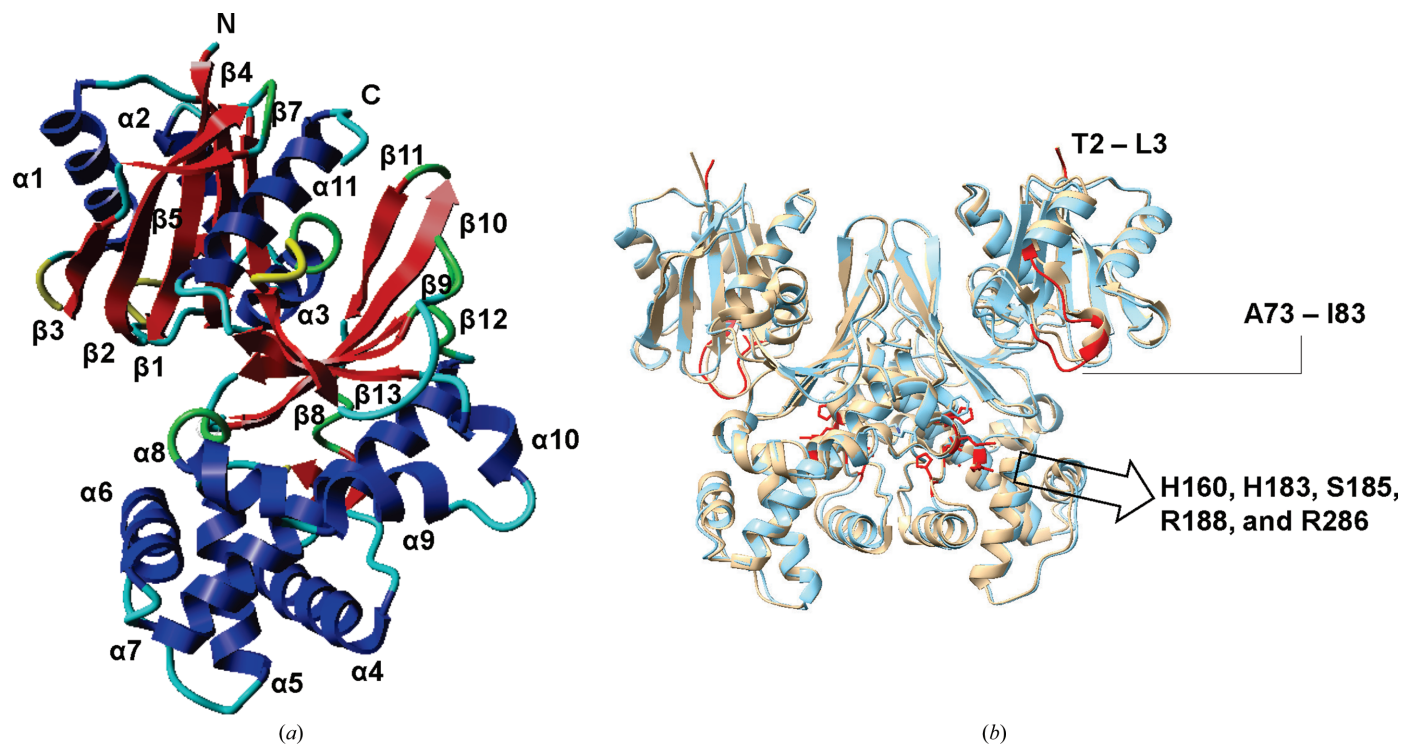


Figure 1
 (a) Secondary-structure mapping of the ecGLK monomer. The model uses a blue color for α -helices and a red color for β -sheets. β_6 is hidden behind because the model is placed in the same direction as in (b) for easy identification. (b) Comparison of the structures of phosphate-bound ecGLK (PDB entry 9duc, cyan) and apo ecGLK (PDB entry 1q18, tan). Sections with the highest observed differences from the B -factor graphing and the r.m.s.d. graphing are highlighted in red.

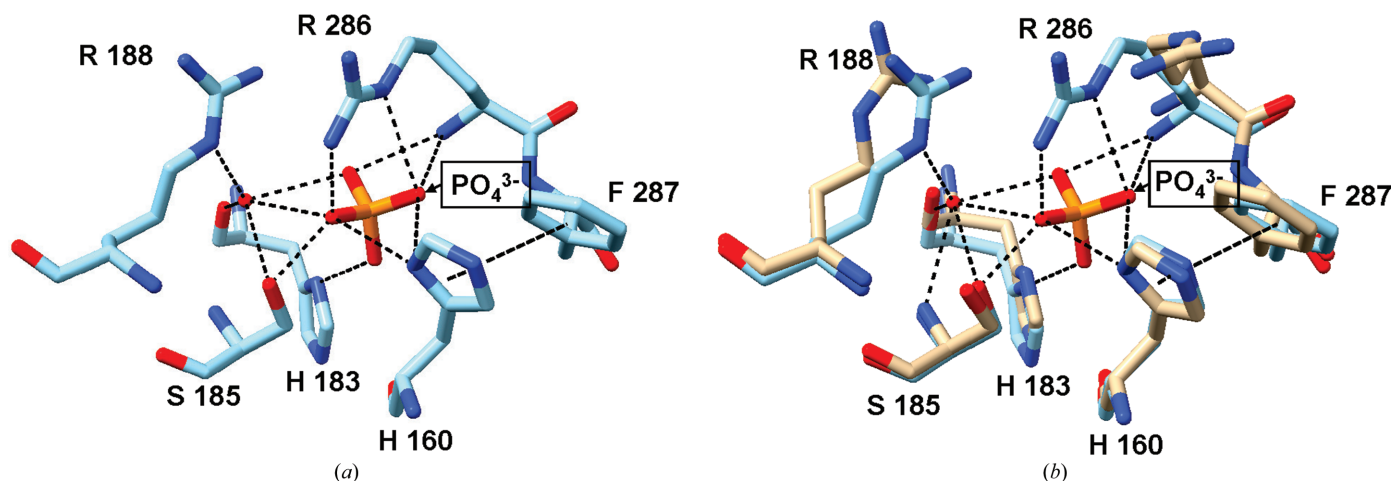


Figure 2

The structure of the phosphate-binding site. (a) Amino-acid residues in the phosphate-binding site. (b) Superimposition of the residues in apo-form ecGLK (PDB entry 1q18, tan) and phosphate-bound ecGLK (PDB entry 9duc, cyan) at the phosphate-binding site.

hydrogen bond to the O atoms (O1 and O4) of the phosphate (Fig. 2). This bond helps to anchor His160 in the active site, while a π -stacking interaction with Phe287 from chain *A* further reinforces this stability. In contrast, His160 is more flexible in the apo form, indicating that binding to phosphate limits its movement. Arg286 is also important for stabilization through phosphate interaction and undergoes significant structural changes upon binding. The guanidinium group of Arg286 moves closer to the phosphate, allowing the formation of several stabilizing hydrogen bonds. Specifically, Arg286 interacts with O1 and O3 of phosphate in chain *A* through its nitrogen (Arg286 N), and its NH₂ group forms hydrogen bonds to O4 of phosphate. Additional interactions between Arg286 NE and phosphate O1 further reinforce this stabilization. In chain *B*, Arg286 similarly forms hydrogen bonds to O1 and O3 of phosphate and Glu187 OE1, indicating its key role in anchoring the phosphate (Fig. 2).

Besides His160 and Arg286, other amino acids also contribute significantly to phosphate interactions. His183,

Ser185 and Glu187 exhibit distinct conformational changes upon phosphate binding. His183 moves closer to phosphate, forming a hydrogen bond to phosphate O4 in chain *A* and phosphate O2 in chain *B*. Ser185 OG establishes a hydrogen bond with phosphate O3. Meanwhile, its backbone interacts with water molecules to maintain stability. Additionally, Glu187 adjusts its position to interact with Arg286 NH₂, losing prior interactions with water. Although Arg188 does not directly interact with phosphate, it plays a supporting role by binding water molecules, forming hydrogen bonds that further stabilize the phosphate-bound complex. All of the abovementioned interactions emphasize the effect of phosphate on the structure and stability of ecGLK. The importance of phosphate binding is evident as it helps maintain structural integrity, enhances hydrogen-bonding networks and could impact the catalytic activity.

3.2. Glucose–ecGLK versus phosphate-bound glucose–ecGLK: structural changes and functional implications

The crystals of the phosphate-bound glucose–ecGLK complex were obtained by soaking ecGLK with 5 mM glucose and were grown in 100 mM bis-Tris pH 6.5, 200 mM magnesium chloride, 25% (w/v) PEG 3350. The crystal structure was determined by molecular replacement and refined to an *R* factor of 0.2034 (*R*_{free} = 0.2580) at a resolution of 2.54 Å. The small and large domains retain the α -helices and β -sheets found in phosphate-bound ecGLK as reported above, while there are domain shifts to account for the glucose binding. The small domain shifts down, closing the binding cleft, and the large domain maintains its relative position with slight shifts into the center of ecGLK.

The phosphate-bound glucose–ecGLK complex crystallizes in a more highly ordered space group (*P*₂₁₂₁₂₁) compared with the phosphate-free form (*P*₁₂₁), suggesting that phosphate binding stabilizes the conformation of ecGLK. When comparing the structure of the glucose–ecGLK complex (PDB entry 1sz2) with the phosphate-bound glucose–ecGLK complex (PDB entry 9dvz), we noticed significant differences,

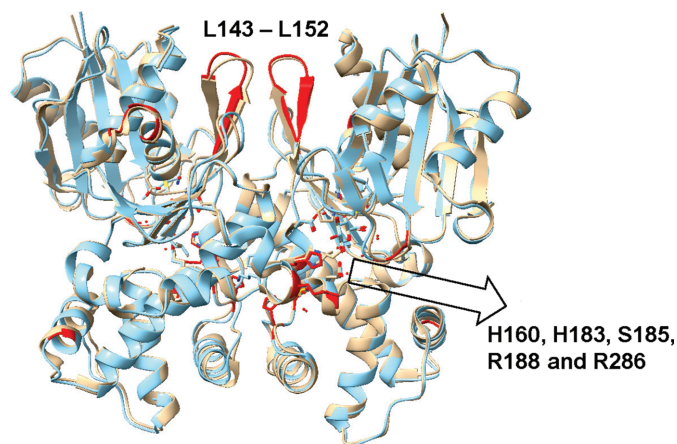


Figure 3

Comparison of the structures of the phosphate-bound glucose–ecGLK complex (PDB entry 9dvz, cyan) and the glucose–GLK complex (PDB entry 1q18, tan). Sections with the highest observed differences from the *B*-factor graphing and the r.m.s.d. graphing are highlighted in red.

especially in loop flexibility and stabilization of the domains (Fig. 3). Residues 108–112 ($\alpha 3$ – $\beta 8$ loop) and 143–152 ($\beta 10$ –loop– $\beta 11$) exhibit notable differences, reflecting conformational shifts upon phosphate binding. Additional structural changes occur in residues 165–173 (loop– $\alpha 4$ helix), 178–182 ($\alpha 4$ helix) and 220–227 ($\alpha 6$ –loop– $\alpha 7$). Residues 313–320 at the tip of the large domain also experience structural divergence, further distinguishing the phosphate-bound glucose–ecGLK complex from the phosphate-free form.

A comparison of *B* factors shows a noticeable decrease in structural flexibility when phosphate binds (Fig. 4). In the glucose–ecGLK complex (PDB entry 1sz2) the average *B* factor is 47.33 Å². It decreases to 27.19 Å² in the phosphate-bound glucose–ecGLK complex (PDB entry 9dvz), suggesting a more rigid structure. Significant differences exist in residues 20–30 (in the $\beta 2$ –loop– $\beta 3$ region), where the interaction changes, possibly due to solvent access. In the glucose–ecGLK complex (PDB entry 1sz2), Cys20 SG forms a hydrogen bond to Asp21 O and water, while in the phosphate-bound glucose–ecGLK complex (PDB entry 9dvz) it retains only the Asp21 O bond. Similarly, Ala23 O in the phosphate-bound glucose–ecGLK complex (PDB entry 9dvz) gains a new hydrogen bond to Arg314 NH₂, stabilizing the loop. Water-mediated inter-

actions in the glucose–ecGLK complex (PDB entry 1sz2), such as those involving Ser24 O, Gly25 O and Glu26 O, are altered or lost in the phosphate-bound glucose–ecGLK complex (PDB entry 9dvz), contributing to its lower *B* factor.

3.3. Glucose and phosphate interactions: phosphate as a potential modulator

When phosphate binds, Arg286 and His160 show conformational changes that affect the stability and hydrogen bonding in the glucose-binding site (Fig. 5). The phosphate binding stabilizes Arg286 and forms hydrogen bonds to the O₂ and O₄ of phosphate in chain *B*. This process reinforces the enzyme structure, lowers its flexibility and may improve glucose binding. His160 maintains hydrogen bonds to glucose while forming new interactions with phosphate in chain *A* (Fig. 6). This dual interaction effectively connects the glucose- and phosphate-binding sites, potentially stabilizing the active site during glucose phosphorylation. These residues also play a critical role in exodomain interactions, stabilizing the enzyme and potentially influencing interactions with other proteins involved in metabolic regulation. Beyond Arg286 and His160, several other structural changes occur upon phosphate

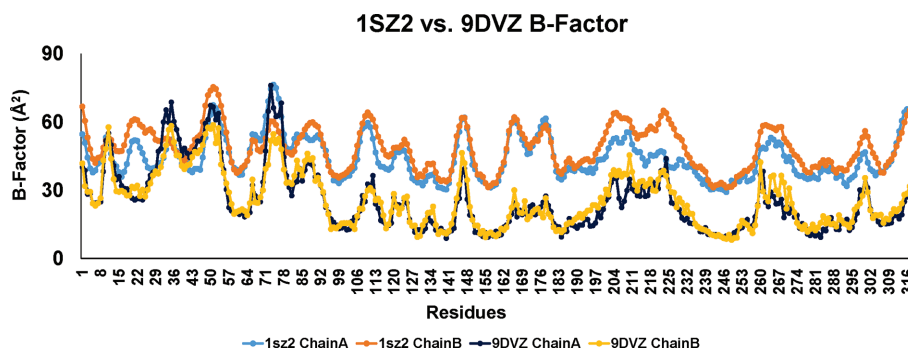


Figure 4
The *B* factors of the structures of the glucose–ecGLK complex (PDB entry 1sz2) and the phosphate-bound glucose–ecGLK complex (PDB entry 9dvz).

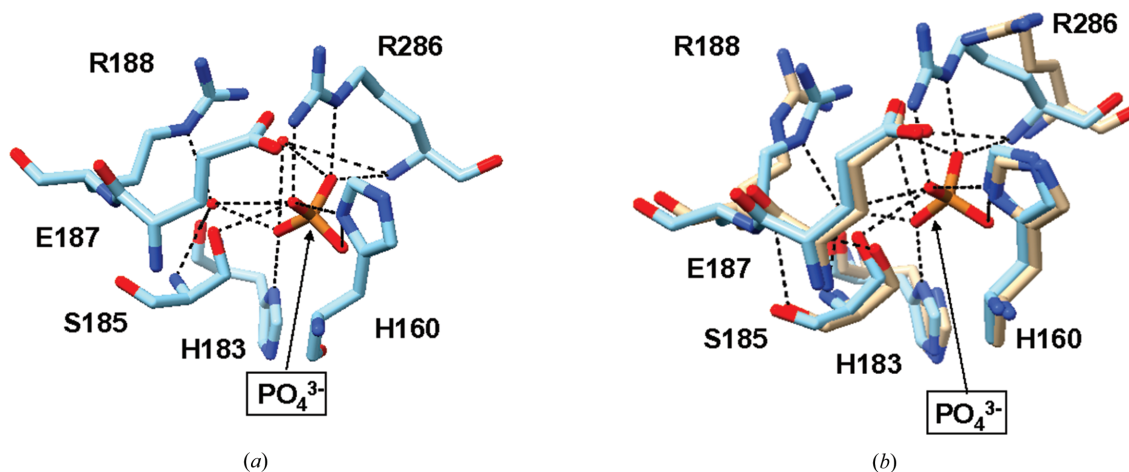


Figure 5
The structure of the phosphate-binding site. (a) Amino-acid residues in the phosphate-binding site. (b) Superimposition of the residues in the glucose–ecGLK complex (PDB entry 1sz2, tan) and the phosphate-bound glucose–ecGLK complex (PDB entry 9dvz, cyan) at the phosphate-binding site.

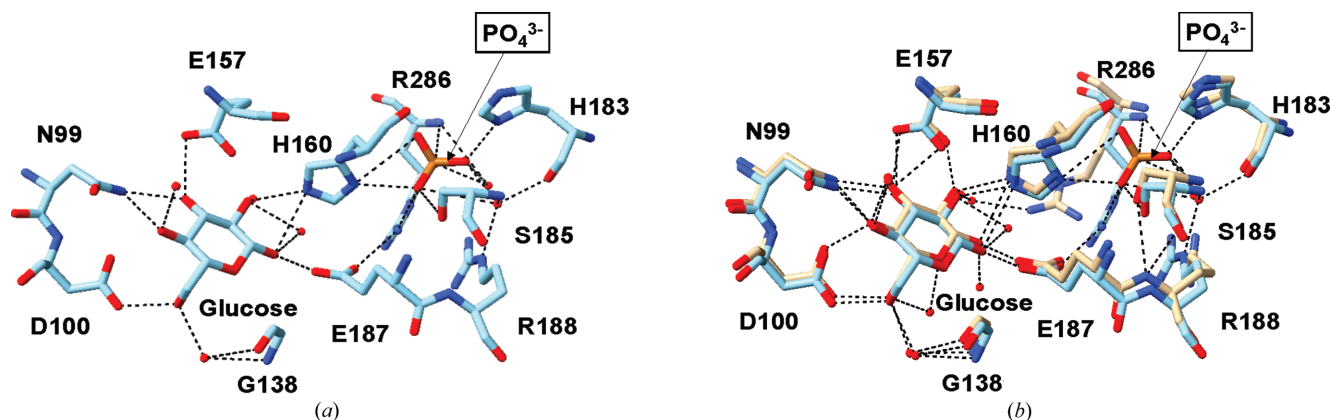


Figure 6

The structure of the glucose- and phosphate-binding sites. (a) Amino-acid residues in the glucose- and phosphate-binding sites. (b) Superimposition of the residues in the glucose-bound complex (PDB entry 1sz2, tan) and the phosphate-bound glucose-bound complex (PDB entry 9dvz, cyan) at the glucose- and phosphate-binding sites.

binding. Key residues such as those at positions 99–101 (within the $\beta 7$ sheet), Gly138 (located in the loop before $\beta 10$) and residues 157–160 (positioned in the loop between $\beta 11$ and $\alpha 4$) show significant differences when comparing phosphate-bound and phosphate-free structures (Fig. 6b). In the phosphate-free structure, the O atom of Glu187 forms hydrogen bonds to both glucose and water, while in the phosphate-bound complex it forms a new hydrogen bond to Arg286 NH₂. This suggests that phosphate indirectly stabilizes glucose binding by modifying hydrogen-bonding patterns and influencing exodomain interactions. Additionally, Ser185 and His183 contribute to these stabilizing effects by forming hydrogen bonds to phosphate, which reduces flexibility and helps to maintain the enzyme conformation during glucose phosphorylation.

Phosphate stabilizes the glucose-binding pocket, primarily through interactions with two key amino acids: His160 and Arg286. His160 forms hydrogen bonds to both phosphate and glucose, linking the phosphate-binding site to the active site and potentially influencing the enzyme activity. Phosphate emerges as a key point of interest due to its abundance in cytosolic conditions, ranging from 1 to 10 mM through various homeostatic mechanisms in *E. coli* (Shulman *et al.*, 1979). The PhoBR two-component signaling system regulates phosphate acquisition and utilization, while excess phosphate leads to polyP accumulation for ATP synthesis (Gardner & McCleary, 2019). Phosphate may impact enzyme activity and enhance the glucose-utilization efficiency. Additionally, enhanced dynamics at the exodomain suggest that GLK regulation may involve protein–protein interactions with other metabolic regulators or signaling proteins.

Data availability

All data created during this research are openly available from the Protein Data Bank under the provided accession numbers.

This study includes the re-analysis of existing data, which are openly available at the locations cited in the references.

Funding information

This research was funded by the National Institutes of Health (grant Nos. R15GM140433 and P20GM139768 to CF) and Arkansas Biosciences Institute.

References

- Afonine, P. V., Grosse-Kunstleve, R. W., Echols, N., Headd, J. J., Moriarty, N. W., Mustyakimov, M., Terwilliger, T. C., Urzhumtsev, A., Zwart, P. H. & Adams, P. D. (2012). *Acta Cryst.* **D68**, 352–367.
- Emsley, P., Lohkamp, B., Scott, W. G. & Cowtan, K. (2010). *Acta Cryst.* **D66**, 486–501.
- Fatema, N., Li, X., Gan, Q. & Fan, C. (2024). *Protein Sci.* **33**, e4845.
- Gardner, S. G. & McCleary, W. R. (2019). *EcoSal Plus*, **8**, 10.1128/ecosalplus.ESP-0006-2019.
- Hansen, T., Reichstein, B., Schmid, R. & Schönheit, P. (2002). *J. Bacteriol.* **184**, 5955–5965.
- Hansen, T. & Schönheit, P. (2003). *FEMS Microbiol. Lett.* **226**, 405–411.
- Lunin, V. V., Li, Y., Schrag, J. D., Iannuzzi, P., Cygler, M. & Matte, A. (2004). *J. Bacteriol.* **186**, 6915–6927.
- McCoy, A. J., Grosse-Kunstleve, R. W., Adams, P. D., Winn, M. D., Storoni, L. C. & Read, R. J. (2007). *J. Appl. Cryst.* **40**, 658–674.
- Meyer, D., Schneider-Fresenius, C., Horlacher, R., Peist, R. & Boos, W. (1997). *J. Bacteriol.* **179**, 1298–1306.
- Ronimus, R. S. & Morgan, H. W. (2004). *Biochem. Biophys. Res. Commun.* **315**, 652–658.
- Sakuraba, H., Goda, S. & Ohshima, T. (2004). *Chem. Rec.* **3**, 281–287.
- Scorpio, D. G., Caspersen, K., Ogata, H., Park, J. & Dumler, J. S. (2004). *BMC Microbiol.* **4**, 1.
- Shulman, R. G., Brown, T. R., Ugurbil, K., Ogawa, S., Cohen, S. M. & den Hollander, J. A. (1979). *Science*, **205**, 160–166.
- Terwilliger, T. C., Grosse-Kunstleve, R. W., Afonine, P. V., Moriarty, N. W., Zwart, P. H., Hung, L.-W., Read, R. J. & Adams, P. D. (2008). *Acta Cryst.* **D64**, 61–69.
- Titgemeyer, F., Reizer, J., Reizer, A. & Saier, M. H. Jr (1994). *Microbiology*, **140**, 2349–2354.